Supplementary Information Appendix

Liquid Metal Enabled Pump

Shi-Yang Tang[a, †], Khashayar Khoshmanesh[a, †,*], Vijay Sivan[a], Phred Petersen[b],

Anthony O'Mullane[c, d], Derek Abbott[e], Arnan Mitchell[a,*] and Kourosh Kalantar-zadeh[a,*]

[a] School of Electrical and Computer Engineering, RMIT University, Melbourne, VIC 3001, Australia

[b] School of Media and Communication, RMIT University, Melbourne, VIC 3001, Australia

[c] School of Applied Sciences, RMIT University, Melbourne, VIC 3001, Australia

[d] School of Chemistry, Physics and Mechanical Engineering, Queensland University of Technology, Brisbane, QLD 4001, Australia

[e] School of Electrical & Electronic Engineering, University of Adelaide, Adelaide, SA 5005, Australia

[†] These authors contributed equally to this work

Corresponding author:

Kourosh Kalantar-zadeh: Tel: +(61 3) 99253254. Email: kourosh.kalantar@rmit.edu.au

Arnan Mitchell: Tel: +(61 3) 99252457. Email: arnan.mitchell@rmit.edu.au

Khashayar Khoshmanesh: Tel: +(61 3) 99252851. Email: khashayar.khoshmanesh@rmit.edu.au

SI Appendix 1: Electrical equivalent circuit of the pump system and the deduction details of Δp.

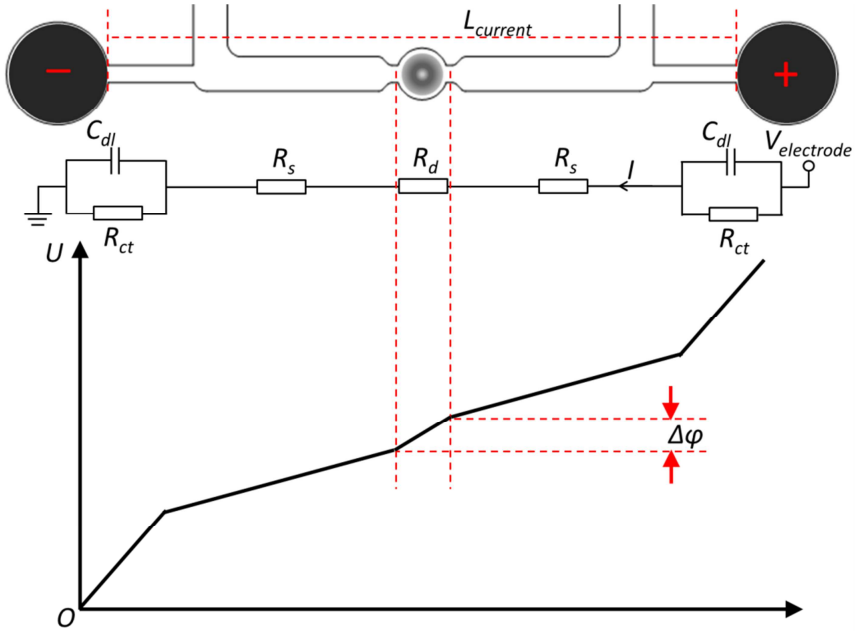

Figure S1. The equivalent circuit describing the pump system: R_s is the electrolyte resistance, R_d is the resistance of the thin layer of electrolyte between the Galinstan droplet and the channel wall. C_{dl} and R_{ct} are the double-layer capacitance and the charge-transfer resistance of the EDL between the graphite electrode and the solution, respectively. $V_{electode}$ is the potential applied between the electrodes, I is the current for the equivalent circuit, and $\Delta\varphi$ is the voltage drop caused by the current flowing through the layer of electrolyte between the Galinstan droplet and channel wall.

Surface tension between the liquid metal and the electrolyte depends on the potential difference across the EDL, as described by Lippman's equation:

$$\gamma = \gamma_o - \frac{1}{2}cV^2 \qquad [S1]$$

where γ is the surface tension, c is the capacitance of the EDL per unit area, V is the potential difference across the EDL, and γ_o is the maximum surface tension when V=0.

Assuming that the charges in the EDL are uniformly distributed in each hemisphere of the Galinstan droplet. Thus, the pressure difference across the EDL at each hemisphere can be obtained from Young-Laplace's equation:

$$p = \gamma \frac{2}{r} \quad \text{[S2]}$$

where p is the pressure difference between the electrolyte and the Galinstan (pressure of Galinstan is higher). Therefore, the pressure difference Δp between the downstream (left) and upstream (right) hemispheres of the droplet can be expressed as:

$$\Delta p = p_L - p_R = (\gamma_L - \gamma_R)\frac{2}{r} = \frac{2\Delta\gamma}{r} \quad \text{[S3]}$$

where p_L and p_R are the pressure difference between the surrounding liquid and the Galinstan of the downstream and the upstream hemispheres, respectively, while γ_L and γ_R are the surface tension of the downstream and the upstream hemispheres, respectively.

Using equation (S1), the surface tension difference $\Delta\gamma$ can be expressed as:

$$\Delta\gamma = \gamma_L - \gamma_R = \frac{c}{2}({V_R}^2 - {V_L}^2) \quad \text{[S4]}$$

where V_L and V_R are the potential difference across the EDL of the downstream and upstream hemispheres, respectively.

The voltage drop between the two ends of the droplet is expressed as $\Delta\varphi$, which is caused by the current flowing through the layer of electrolyte between the Galinstan droplet and channel wall (Fig. S1). This voltage drop can be estimated as:

$$\Delta\varphi = IR_d \approx I\frac{2r}{\sigma A_{gap}} \approx \frac{\sigma V_{electrode} A_{current}}{L_{current}} \frac{2r}{\sigma A_{gap}} \quad \text{[S5]}$$

$$= \frac{2V_{electrode}\, A_{current} \cdot r}{L_{current}\, A_{gap}}$$

where I is the current in the circuit, σ is the conductivity of the electrolyte, A_{gap} is the equivalent cross sectional area of the electrolyte between the Galinstan droplet and channel wall in the droplet seat chamber, $V_{electrode}$ is the potential applied between the electrodes, $L_{current}$ is the total length of the current path, and $A_{current}$ is the equivalent cross sectional area of the current path. If the value of the droplet radius r is close to the radius of the droplet seat chamber (1.5 mm), A_{gap} can be estimated as:

$$A_{gap} \approx \frac{v_{seat} - \frac{4}{3}\pi r^3}{2r} = \frac{v_{seat}}{2r} - \frac{2}{3}\pi r^2 \qquad \text{[S6]}$$

where v_{seat} is the volume of the electrolyte in the droplet seat chamber. According to equation (S6), we see that larger r leads to smaller A_{gap}. In the presence of no external potential applied, the EDL is initially charged by q_o and the voltage that appears due to this charge is V_o, which can be expressed as: $V_o = q_o/c$. The potential difference across the EDL and the absolute voltage can be related as: (1)

$$\mathrm{V}_L = V_o - \frac{\Delta\varphi}{2} \qquad \text{[S7]}$$

$$\mathrm{V}_R = V_o + \frac{\Delta\varphi}{2} \qquad \text{[S8]}$$

Inserting the values of V_L and V_R into equation (S4), the surface tension difference $\Delta\gamma$ can be calculated as:

$$\Delta\gamma = \mathrm{c}V_o \cdot \Delta\varphi = q_o \cdot \Delta\varphi \qquad \text{[S9]}$$

By combining Eqs. **S2** to **S9**, the pressure difference Δp can be expressed as:

$$\Delta p = \frac{2\Delta\gamma}{r} = \frac{2q_o \cdot \Delta\varphi}{r} = \frac{4q_o\, A_{current} \cdot V_{elctrode}}{L_{current}\ A_{gap}} \quad \text{[S10]}$$

If we assume q_o=0.05 C/m^2 (2), $A_{current}$= 5 mm^2, $V_{electrode}$=2.5 V, $L_{current}$=40 mm, A_{gap}=4 mm^2 (when r=1.35 mm), the value of Δp is estimated as 15.5 Pa. This is a sufficient pressure drop to produce a pumping effect.

SI Appendix 2: Detailed explanation of the pumping mechanism

Moving droplet:

Applying an external potential along the channel leads to redistribution of the charges in the EDL along the surface of the Galinstan droplet, as shown in Fig. S2-A. This results in a higher surface tension on the downstream (left) hemisphere of the droplet, as explained in the main manuscript. This in turn increases the pressure difference between the droplet and the surrounding liquid, which is more intense on the downstream hemisphere of the droplet, as shown in Fig. S2-B.

The theoretical variation of pressure across the liquid metal droplet and the surrounding medium has been plotted in Figure S2-C. The plot can be divided into three distinct sections, covering: (i) the liquid metal droplet itself, (ii) the buffer zone, containing the medium in the direct contact with the liquid metal, with sharp variations of velocity and pressure across this zone (note that the size of the buffer zone is exaggerated), and (iii) the medium far from the droplet.

Across the liquid metal droplet, the pressure difference reaches its maximum at the downstream end and reduces towards the upstream end of the droplet, as discussed before. Across the buffer zone, the pressure sharply reduces until becoming zero on both sides of the moving liquid metal droplet.

The pressure difference between the droplet and the medium produces counteracting forces of $F_L^{'}$ and $F_R^{'}$ on the droplet along the *x*-axis, as shown in Fig. S2-D. $F_L^{'}$ is larger due to higher pressure generated at the downstream hemisphere (left). As a result, the droplet is pushed towards the upstream (right) direction.

The motion of the droplet system can be interpreted with the analogy of a motion of a rowing boat on the water, as shown in Fig S2-E. The Galinstan droplet is similar to the boat where the pressure difference produced across the pump generates a force similar to that of produced by the paddles.

When the paddle moves in the direction of the black arrow (Figure 2S-E), a higher pressure is produced on the left-hand side of the paddle, which pushes the boat towards the right-hand side.

Stationary droplet (pumping liquid):

The blocking of the Galinstan droplet by the neck of the droplet seat chamber does not change the distribution of charge in the EDL or the pressure on the surface (Fig. S2-A' and B'). This is because the voltage drop between the two ends of the droplet $\Delta\varphi$ remains the same. Additionally, as evidenced by the images shown in Fig. S2-B", the deformation of the droplet is minimal, i.e. $(D_1/D_{initial} - 1)\times 100\% = 2.6\%$, and its contact area with the neck of the seat chamber is much smaller than the droplet surface area itself. In the other words, the overall pressure on the left hemisphere of the droplet is always larger than that of the right hemisphere as along as an external potential is applied. As a result, the variations of pressure across the liquid metal droplet remain the same as the case when the droplet was moving to the right side (Fig. S2-B').

Along the channel, the pressure reduces linearly according to the direction of the flow (this linear reduction in pressure is due to the effect of wall shear stress) (3). Across the buffer zone, the pressure sharply changes (reduces at the far left while increases at the far right) to match the pressure of the flow with that of the liquid metal droplet (Fig. S2-C').

The droplet is held still by the chamber as the overall force on the droplet is zero, as the force produced by the pressure difference across the hemispheres and the force applied by the seat chamber reach a balance. In this case, the pressure difference across the droplet causes the flow of the surrounding liquid towards left, as shown in Fig. S2-D'.

As soon as the droplet is constrained by the wall of the droplet seat chamber, the Galinstan droplet is deformed and a smaller radius of curvature is formed on the upstream of the droplet. As a result, the resultant forces induced by the pressure difference between the Galinstan droplet and the surrounding liquid, as well as the neck of the chamber, is balanced, as described below and shown in Fig. S2-D':

$$F_L - F_R = F_{Wall} = \dot{m}\, U_{liquid}$$

$$\rightarrow\ P_L \times A_L - P_R \times A_R = F_{Wall} > 0$$

$$A_L \approx A_R\ \rightarrow\ P_L - P_R > 0$$

where $\dot{m}$ is mass flow rate and U_{liquid} is the average velocity of the liquid, P_L and P_R are the pressure difference between the droplet and the surrounding liquid on the downstream and upstream hemisphere of the droplet, respectively. A_L and A_R are the surface area of the downstream and upstream hemispheres of the droplet, respectively. As P_L is larger than P_R, which is not balanced, a flow of liquid is induced.

Similarly, the induced flow can be interpreted using a rowing boat analogy, where the paddle is moving but the boat is stopped by an impeding block, as shown in Fig. S2-E'. The high pressure produced on the left-hand side of the paddle cannot move the boat and instead generates the flow of the surrounding liquid towards the left side.

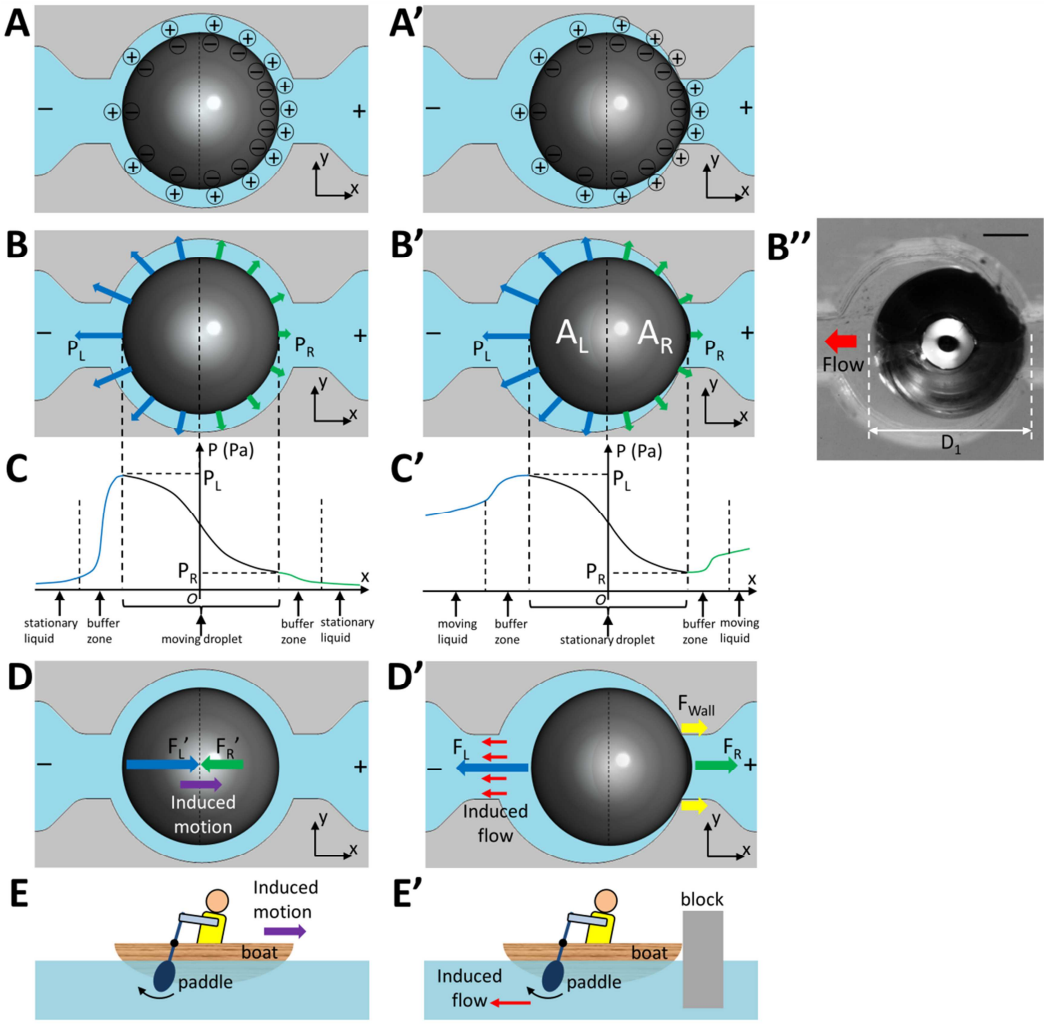

Figure S2. Operation mechanism of the liquid metal enabled pump.

Moving droplet: (*A*) Schematic of the Galinstan droplet EDL charge distribution when an electric field is generated between the graphite electrodes. (*B*) Pressure distribution along the Galinstan droplet surface. (*C*) Variations of pressure along the channel. (*D*) Counteracting forces applied by the surrounding liquid on the Galinstan droplet along the *x*-axis. (*E*) Schematic of a rowing boat as an analogy to the Galinstan droplet.

Stationary droplet (pumping liquid): (*A'*) Schematic of the Galinstan droplet EDL charge distribution. (*B'*) Pressure distribution along the Galinstan droplet surface. (*C'*) Variations of pressure along the channel. (*B''*) A Galinstan droplet is constrained in a droplet seat chamber. Scare

bar is 1 mm. (*D'*) The Galinstan droplet motion is stopped by the seat chamber neck and the pressure difference generates a flow of surrounding medium. (*E'*) Schematic of a rowing boat as an analogy to the pumping system.

SI Appendix 3: Raman spectra of the Galinstan droplet surface

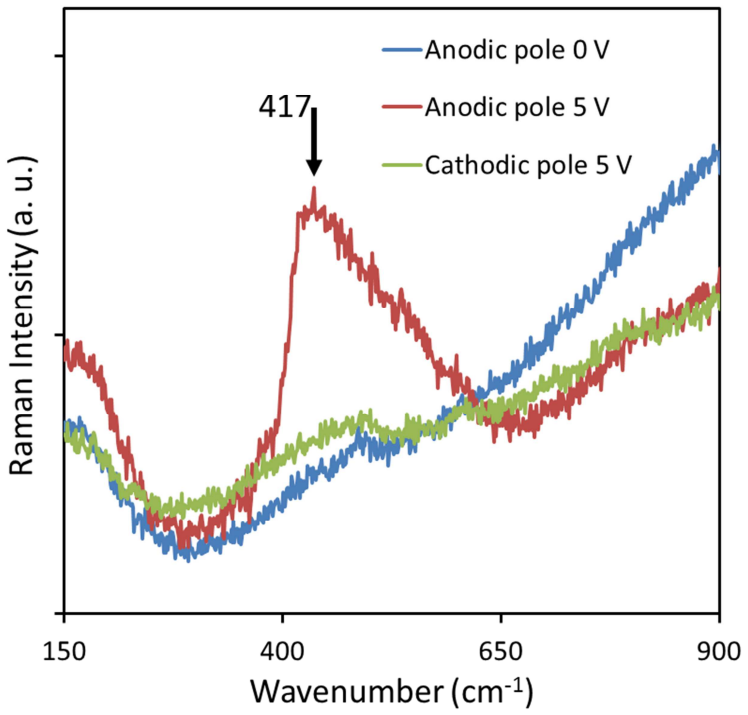

Figure S3. Raman spectra of the Galinstan droplet in the 150–900 cm^{-1} region at 0 and 5 V. An electrochemical reaction takes place when the Galinstan droplets are polarised upon the application of an electric field. A series of Raman measurements is conducted (while the liquid metal is held still in a reservoir). As can be seen, a β-Ga_2O_3 layer is formed on the anodic pole of the droplet surface (as depicted by the appearance of 417 cm^{-1} peak shift) (4) when a +5 V DC voltage is applied between the two electrodes. This oxide layer changes the properties of the electrical double layer which assist the electrowetting/de-electrowetting process during the application of the pulses.

SI Appendix 4: Sequential snapshots demonstrating the pumping effect of a Galinstan droplet when a 5 V DC voltage applied

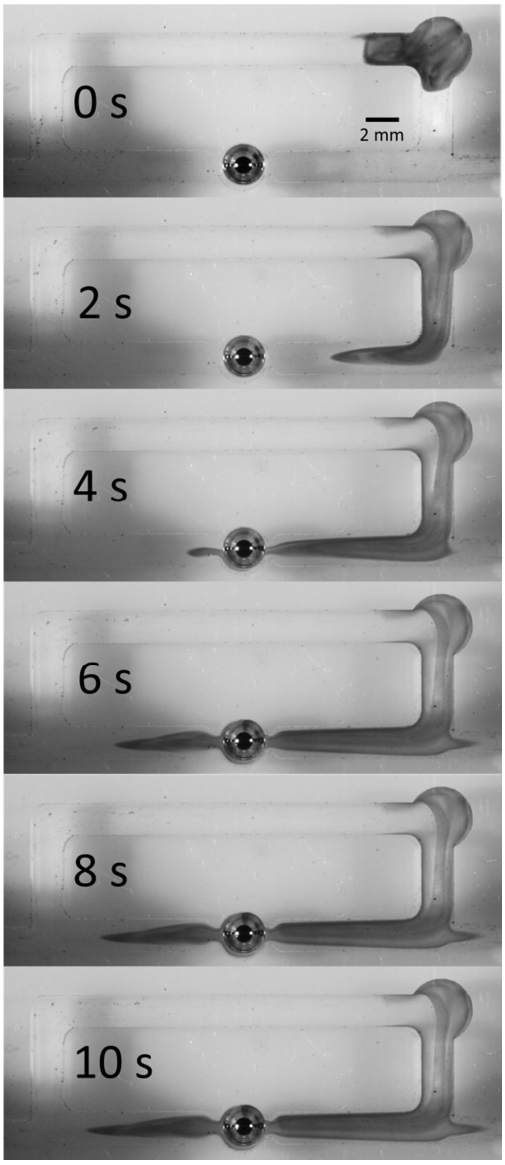

Figure S4. Sequential snapshots for the pumping effect of a Galinstan droplet with 2.7 mm diameter in the PMMA channel filled with NaOH solution (0.3 mol/L), while a 5 V DC voltage is applied between the two graphite electrodes, a droplet of dye is used to demonstrate the pumping effect. The pumping effect is diminished and finally vanishes after 6 s.

SI Appendix 5: High speed images of the droplet.

Using a high speed camera (2000 frame/s), sequential snapshots for a Galinstan droplet during one cycle of the applied voltage signal when a 5 $V_{p\text{-}p}$, 200 Hz square wave with 2.5 V DC offset is applied, as shown in Fig. S5. The droplet locates at the right-hand side of the chamber and slightly protrudes into the neck of the channel. However, no further obvious change of droplet morphology and no oscillatory movement is observed, indicating that the pumping effect is not caused by droplet oscillation.

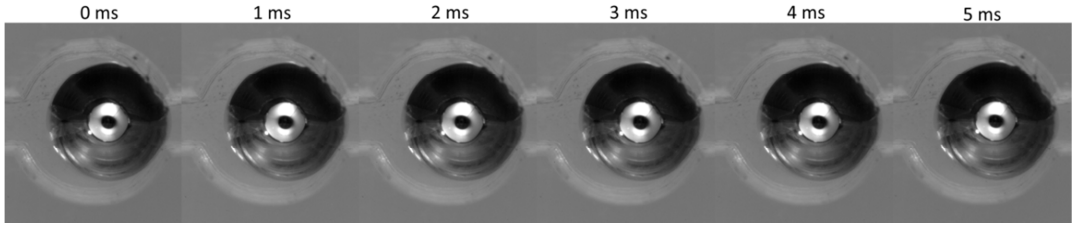

Figure S5. Sequential snapshots for the Galinstan droplet during one signal cycle.

The potential across the EDL at the interface between the metal droplet and electrolyte increases towards the upstream hemisphere causing a gradient in interfacial tension (Fig. S2-A). The interface is thus should drawn towards the downstream hemisphere, by a phenomenon similar to continuous electrowetting (Eq. 1), or the Marangoni effect. Under electrostatic conditions, the interface would distort to minimize surface energy and terminate once equilibrium was achieved. However, it is clear from our observations (Fig. S5 and S2-B") that pumping continues even after deformation has ceased. To explain this, one could imagine the electric current flowing through the electrolyte as a stream of ions. The ions impact the downstream hemisphere, neutralizing the EDL and releasing the fluid from both sides of the interface. Continuous electrowetting may then push the released electrolyte downstream, away from the droplet and the liquid metal can recirculate through the body of the droplet to the upstream hemisphere, forming eddies.

SI Appendix 6: Control experiments without Galinstan droplet and with Mercury droplet.

In order to rule out the electro-osmosis effect, a control experiment is conducted without liquid metal droplet in place. No pumping effect is observed, using a square wave signal of 200 Hz, 16 V_{p-p}, 8 V DC offset and 50% duty cycle, as indicated by injecting a droplet of dye (Fig S6-A). Increasing the magnitude of the voltage leads to electrolysis of the solution with gas bubbles generated on the electrodes while no pumping occurs. Adding a Galinstan droplet into the chamber after 7 s leads to immediate pumping of the liquid (Fig. S6-A).

We also conduct a control experiment with a mercury droplet instead of Galinstan. A flow rate of 1,500 µL min^{-1} is obtained using a square wave signal of 200 Hz, 5 V_{p-p}, 2.5 V DC offset and 50% duty cycle, which is comparable to the performance of Galinstan droplet (Fig S6-B). This confirms that the pumping of liquid is caused by the electrowetting effect.

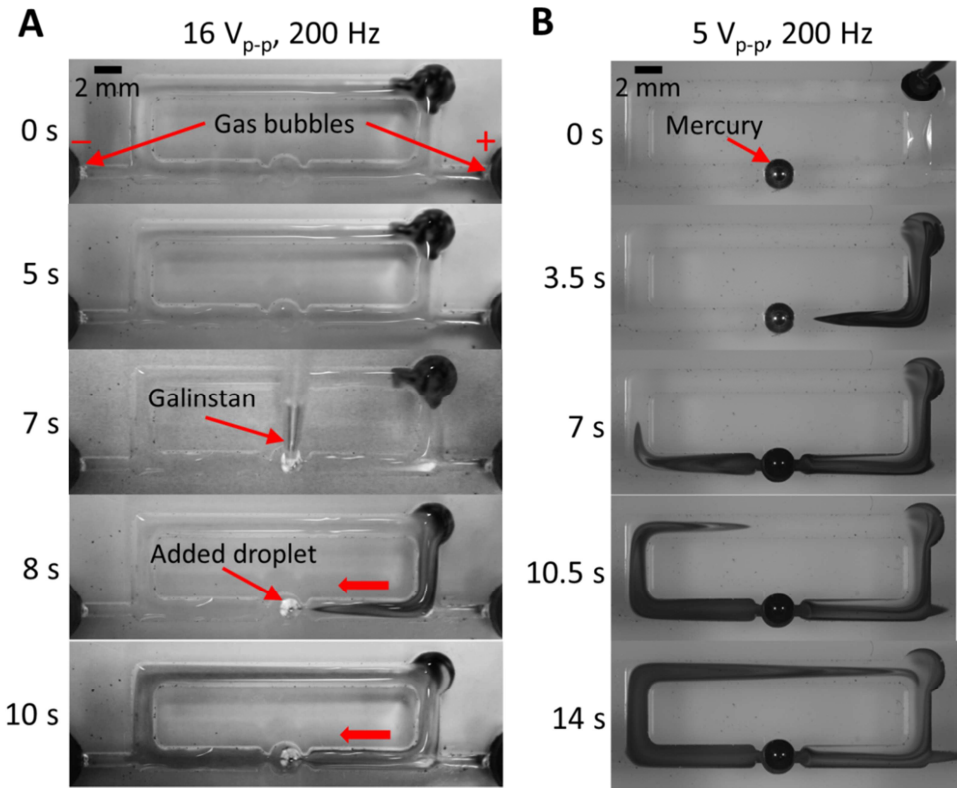

Figure S6. Experiments without liquid metal and with mercury droplets. (*A*) Sequential snapshots for the pumping effect with and without a Galinstan droplet in the PMMA channel filled with NaOH

solution (0.3 mol/L). The Galinstan droplet is added at 7 s. A square wave signal (200 Hz, 16 V_{p-p}, 8 V DC offset and 50% duty cycle) is applied between the two graphite electrodes. (*B*) Sequential snapshots for the pumping effect of a mercury droplet with 2.7 mm diameter in the PMMA channel filled with NaOH solution (0.3 mol/L), while a square wave signal (200 Hz, 5 V_{p-p}, 2.5 V DC offset and 50% duty cycle) is applied. Droplets of dye are used for demonstrating the pumping effect. Scale bar is 2 mm.

SI Appendix 7: Calculation of Galinstan droplet lifetime.

Inductively coupled plasma mass spectrometry (ICP-MS) tests indicate that the gallium concentration is increased from 0.15 to 71.34 μmol/L in 20 min (~100 cycles). The molecular mass of gallium is 69.723 g/mol and the volume added to the channel is 0.4 mL. Therefore, the amount of gallium loss can be estimated as below:

$$Gallium\ loss = \frac{(71.34 - 0.15)\mu mol/L}{10^6} \times 69.723\ g/mol \times \frac{0.4\ mL}{1000\ mL} = 1.985\ \mu g$$

The density of Galinstan is 6.44 g/cm^3 (5) and it contains 68.5% of gallium. If the weight percentage of gallium reduces from 68.5% to 59.6%, the Galinstan droplet will lose its eutectic ability (6). Thus the life time of one droplet of Galinstan of 2.7 mm diameter can be estimated as:

$$Life\ time\ of\ Galinstan\ droplet =$$

$$(6.44\ \mathrm{g}/cm^3 \times \frac{4}{3}\pi \times 0.135^3) \times (68.5\% - 59.6\%) \times \frac{20\ min}{1.985\ \mu g} \approx 59516\ min \approx 41\ days$$

Here we have ignored the effect of tin since the amount of tin dissolved in the solution is small compared to gallium.

SI Appendix 8: Computational fluid dynamic (CFD) simulations

A series of CFD simulations are conducted to comprehend the behaviour of the soft pump using the ANSYS Fluent 6.3 Software Package (Canonsburg, PA, USA). The simulations are conducted in 3D and steady state. The fluid is assumed to be Newtonian and the flow is considered laminar due to its low Reynolds number. Under these conditions, we solve the Navier-Stokes differential equations governing the balance of mass and momentum for the liquid flowing inside the poly(methyl methacrylate) (PMMA) channel, as given below:

$$\nabla \cdot \vec{U} = 0 \qquad \text{[S11]}$$

$$\rho\,(\vec{U} \cdot \nabla)\,\vec{U} = -\nabla P + \mu\,\nabla^2 \vec{U} \qquad \text{[S12]}$$

in which $\vec{U}$ and P are the velocity and pressure, respectively, while ρ = 998 kg/m^3 and μ = 0.001 Pa·s are the density and dynamic viscosity of the liquid.

The boundary conditions include a constant shear stress along the upstream side of the soft pump, a zero shear stress along the top free surface of the channel and no-slip boundary condition along the other surfaces of the channel. The pressure difference along the downstream and the upstream hemispheres of the droplet (Δp) presented in Equation (1), can be translated into a constant shear stress (τ) across the entire surface of the droplet:

$$\Delta p \cdot A_{cross\ section} = \tau \cdot A_{surface\ area}$$

$$\Rightarrow \quad \Delta p \cdot \pi\, r^2 = \tau \cdot 4\,\pi\, r^2 \quad \Rightarrow \quad \tau = \Delta p/4 \qquad \text{[S13]}$$

Moreover, the Lagrangian particle tracking model is utilized to predict the trajectory of particles suspended in the liquid as:

$$\frac{d\vec{U}_{\text{particle}}}{dt} = \frac{18\mu}{\rho_{\text{particle}} D^2_{\text{particle}}}(\vec{U}_{\text{embyo}} - \vec{U}) + (\rho_{\text{particle}} - \rho) g_z \qquad \text{[S14]}$$

where $\vec{U}_{\text{particle}}$, ρ_{particle} and D_{particle} are the velocity, density and diameter of the suspended particles, respectively.

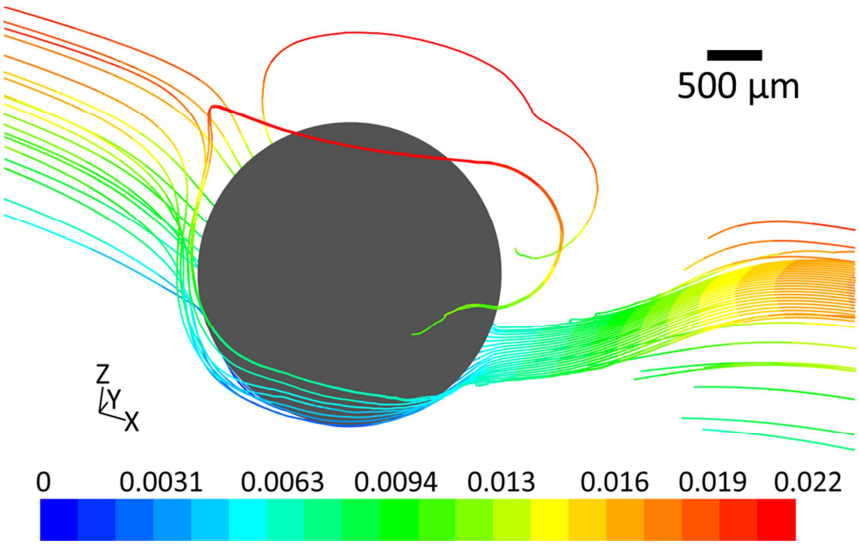

Figure S8. The trajectory of suspended particles coloured by the velocity of particles (m/s) and obtained by the Lagrangian particle tracking model. The particles follow the pattern of the vortices, as shown in Fig. 2B in the main manuscript, move downward to pass through the interface of the two vortices.

SI Appendix 9: Schematics of the developed PMMA channels with shorter electrode gaps

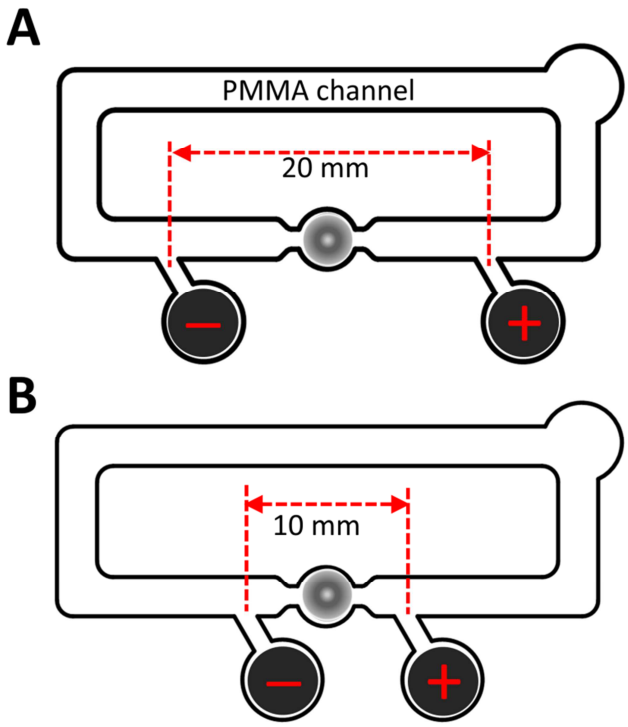

Figure S9. Schematic of the PMMA channel with the gap between the electrodes of (*A*) 20 mm and (*B*) 10 mm. The length of the channel is 65 mm.

SI Appendix 10: Schematic of current flow.

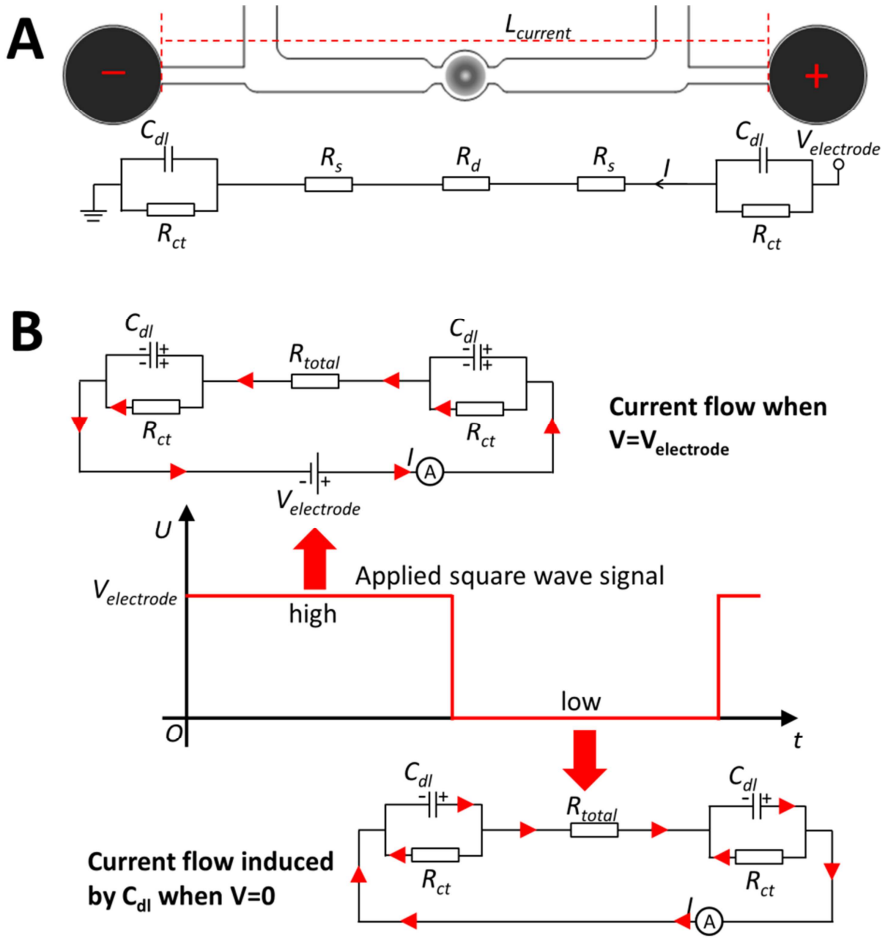

Figure S10. (*A*) The equivalent circuit describing the pump system: R_s is the electrolyte resistance, R_d is the resistance of the thin layer of the electrolyte between the Galinstan droplet and the channel wall. C_{dl} and R_{ct} are the double-layer capacitance and the charge-transfer resistance of the EDL between the graphite electrode and the solution, respectively.

(*B*) Schematic for current flow in the circuit when the square wave signal as shown is applied, where $R_{electrolyte}=2R_s+R_d$. When the signal is high, the current is positive and C_{dl} is charged. When the signal is low, C_{dl} starts discharging and the current becomes negative. The arrows in the circuits show the direction of the current.

SI Appendix 11: Pump performance using a close-top channel.

Experiments are conducted using a close-top channel with the same dimensions as the one shown in Fig. S11. Channel 3 is used which the gap between the graphite electrodes is 10 mm, a glass slide is applied to cover the top of the channel. The channel is filled with NaOH solution (0.3 mol/L). A square wave signal (200 Hz, 5 V_{p-p} with 2.5 DC offset and 50% duty cycle) is applied. No noticeable change is observed in the performance of the pump, and a flow rate of 5,400 μL/min is achieved, as shown in Fig. S11.

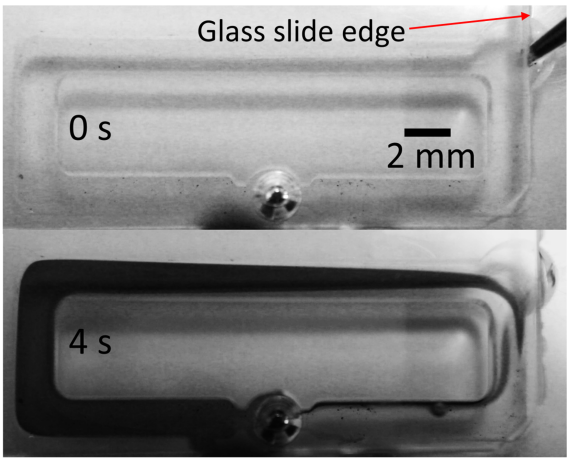

Figure S11. Operating the pump using a close-top channel.

SI Appendix 12: Schematics of the developed PMMA channels with longer loop length.

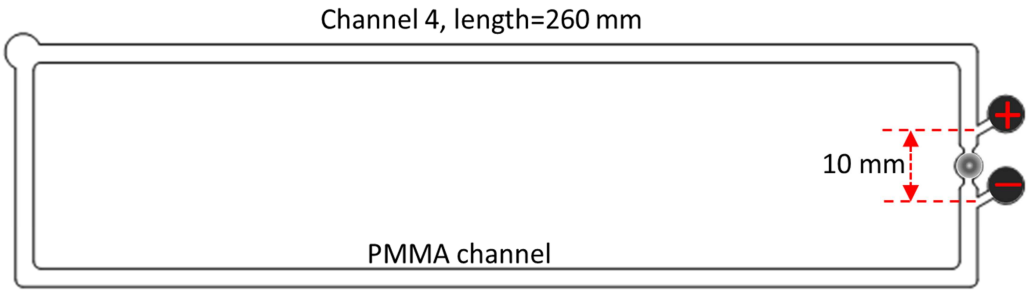

Figure S12. Schematic of the Channel 4, the electrode gap is kept at 10 mm and length of the channel is extended to 260 mm.

SI Appendix 13: Pump performance characterization with respect to different duty cycles and waveforms.

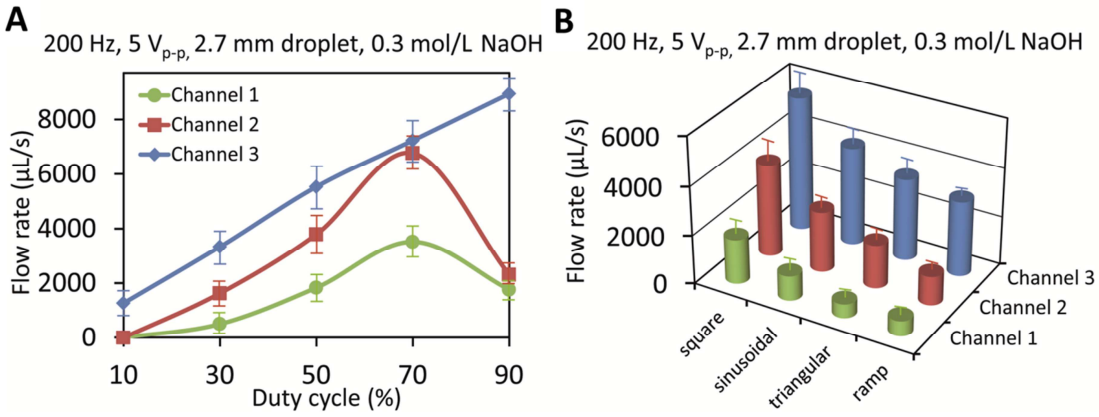

Figure S13. (*A*) Plot of flow rate *vs* duty cycle when a 200 Hz, 5 V_{p-p} square wave signal is applied, obtained with a 2.7 mm diameter Galinstan droplet in a 0.3 mol/L NaOH solution. For Channels 1 and 2, the flow rate reaches the maximum at the duty cycle of 70%, this can be attributed the oxidation of the downstream hemisphere of the droplet when duty cycle is large, which is similar to the case when a DC voltage is applied as shown in Supplementary Figure S4. However, for the small electrode gap design (Channel 3), the pressure difference Δp generated is large due to small $L_{current}$, and the pumping performance is less affected by the oxidation of the droplet. (*B*) Plot of flow rate *vs* wave shape for all three channels when a 200 Hz, 5 V_{p-p} square wave signal is applied, obtained with a 2.7 mm diameter galinstan droplet in a 0.3 mol/L NaOH solution. At such a condition, square wave provides the highest flow rate, while the ramp voltage gives the smallest flow rate.

SI Appendix 14: Flow rate-square wave frequency plots for Galinstan droplets with different diameters.

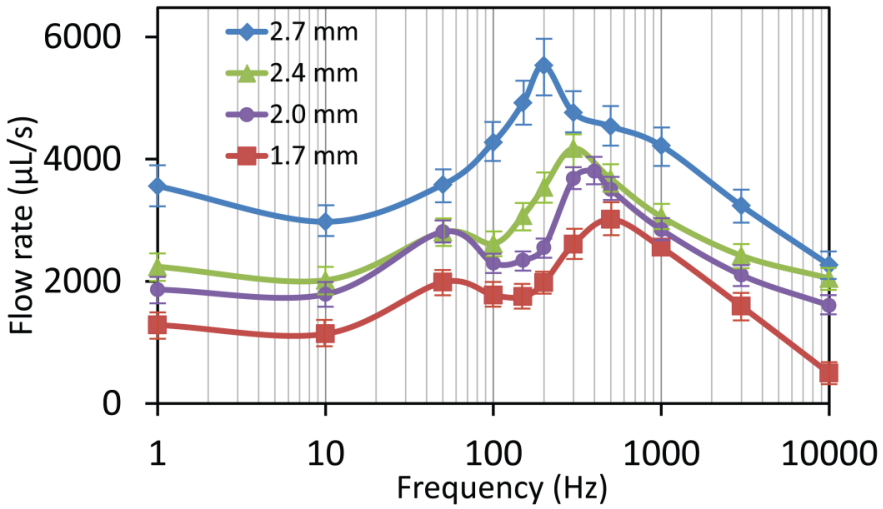

Figure S14.a. Plot of flow rate *vs* square wave frequency, obtained with Galinstan droplets of different diameters in Channel 3 (10 mm electrode gap) filled with 0.3 mol/L NaOH solution. The optimised frequency increases from 200 Hz to 500 Hz by decreasing the diameter of the droplet form 2.7 mm to 1.7 mm. Obviously, the smaller the surface the faster the electrowetting/de-electrowetting occurs which results in larger resonance frequencies.

For Galinstan droplets with the diameters smaller than 2.7 mm, there is an additional peak at 50 Hz. Mechanical oscillation within the reservoir can be observed for Galinstan droplets with the size smaller than 2.7 mm within the droplet seat and this may provide mechanical pumping effect, the size of the reservoir perhaps is responsible to this fix 50 Hz resonance.

The shoulder of peaks observed at very low frequencies (< 1 Hz) is probably due to the elongation of the droplet caused by the deformation, as shown in Fig. S14.b. This may increase the pressure difference between the both sides of the droplet.

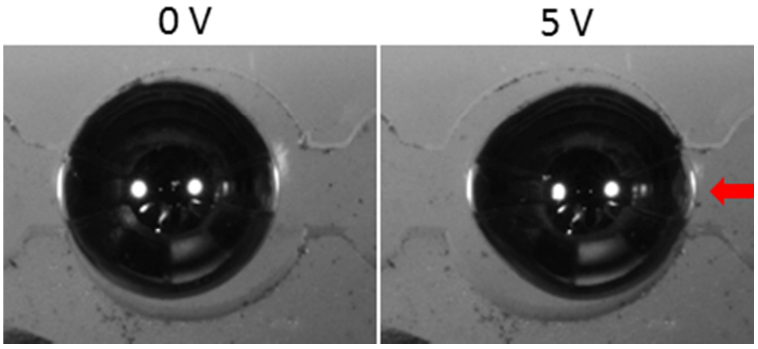

Figure S14.b. Deformation of Galinstan droplet when the applied square signal reaches the peak voltage (5 V).

SI Appendix 15: Pump curve

In order to change the pressure drop along the channel, we fabricated a customized gate valve, as shown in Fig. S15.a. Turning the screw leads to the changing of cross sectional area of the channel at the location of the screw seat, which in turn, changes the pressure drop.

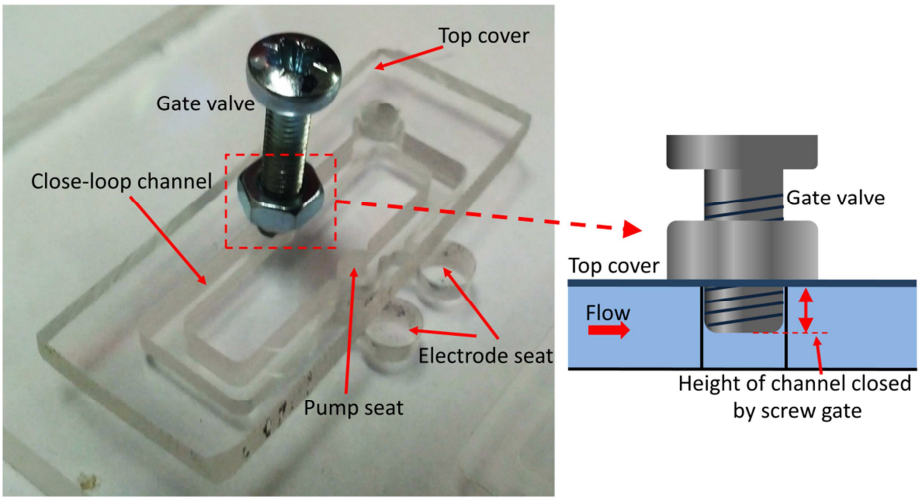

Figure S15.a. Custom-built gate valve to induce desired pressure drops along the channel.

Results are obtained using 0.3 mol/L NaOH solution pumped by a Galinstan droplet of 2.7 mm diameter using a 6 $V_{p\text{-}p}$, and 50% duty cycle with 3 V DC offset square wave signal at the frequencies of 10, 200 and 1000 Hz (Fig. S15.b-A). 6 $V_{p\text{-}p}$ is the maximum operating voltage for 0.3 mol/L NaOH solution without electrolysing the electrolyte. Simulations are conducted to obtain the flow rate and pressure drop at each condition. Flow rates obtained by the simulations have a good agreement with experimental values. The calculated pump curve is shown in Fig. S15.b-B. The boundary conditions are adjusted by implementing a scale factor in Eq. **1** in the main manuscript to represent the influence of applied signal frequency. In this case, the actual pressure difference produced by the pump can be obtained using: $\Delta p = \Delta p_{max} \cdot k(frequency)$, where Δp_{max} is obtained by Eq. **1** and $k(frequency)$ is obtained from Fig. 3C in the main manuscript.

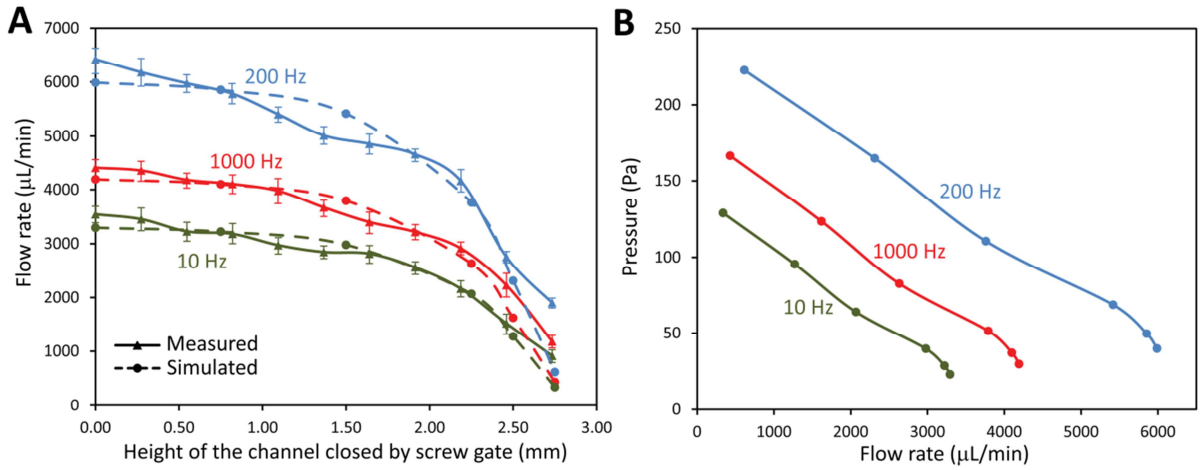

Figure S15.b. (*A*) Flow rate *vs* screw gate position plot, measured values are obtained using 0.3 mol/L NaOH solution pumped by a Galinstan droplet with 2.7 mm diameter using a 6 $V_{p\text{-}p}$, and 50% duty cycle with 3 V DC offset square wave signal at the frequencies of 10, 200 and 1000 Hz. (*B*) Calculated pump curve at 10, 200 and 1000 Hz operating frequencies.

SI Appendix 16: Pump performance characterization with liquids of high viscosities

The performance of the system for pumping liquids of high viscosities is investigated. The viscosity of the working liquid (8.93×10^{-4} Ns/m^2) is increased by adding DI water to glycerol with the mixing ratios (*v/v*) of 1:1, 1:3 and 1:9 (water : glycerol) in order to obtain viscosities of 6.88×10^{-3}, 0.0415, and 0.209 Ns/m^2, respectively. The corresponding viscosity is calculated based on the parameters in (7) at room temperature. NaOH is added to the water-glycerol solutions to obtain a concentration of 0.3 mol/L. Channel 3 is used, in which the gap between the graphite electrodes is 10 mm. Applying a square wave signal of 200 Hz, 5 V_{p-p}, 2.5 V DC offset and 50% duty cycle leads to flow rates of 4,700, 2,400 and 200 µL/min with water-glycerol solutions of 1:1, 1:3 and 1:9 (water : glycerol) volumetric ratios, respectively (Fig. S16-A). Flow rate is reduced when the viscosity of the liquid increases (Fig. S16-B). The results show that the liquid metal enabled pump is able to pump liquids, which are ~230 times more viscous than DI water.

We also investigate the performance of the system for pumping a high viscosity liquid, with a high density of suspended particles. Water-glycerol solution with the mixing ratio of 1:3 (viscosity of 0.0415 Ns/m^2) is used, while polystyrene particles of 10 µm diameters are added into the solution to obtain a concentration of 25 mg/mL (corresponding to ~6×10^6 particle/mL). Applying a square wave signal of 200 Hz, 5 V_{p-p}, 2.5 V DC offset and 50% duty cycle, leads to a flow rate of 2,300 µL/min, which is slightly lower than that of the same solution without particles (Fig. S16-B) (see Supplementary Movie 8, a droplet of dye is added to show the pumping direction). This can be attributed to the increased viscosity of the solution after adding the particles. The diameter of 10 µm is not an upper limit, but provides confidence that the pump could be used with suspensions of most micro-particles of interest.

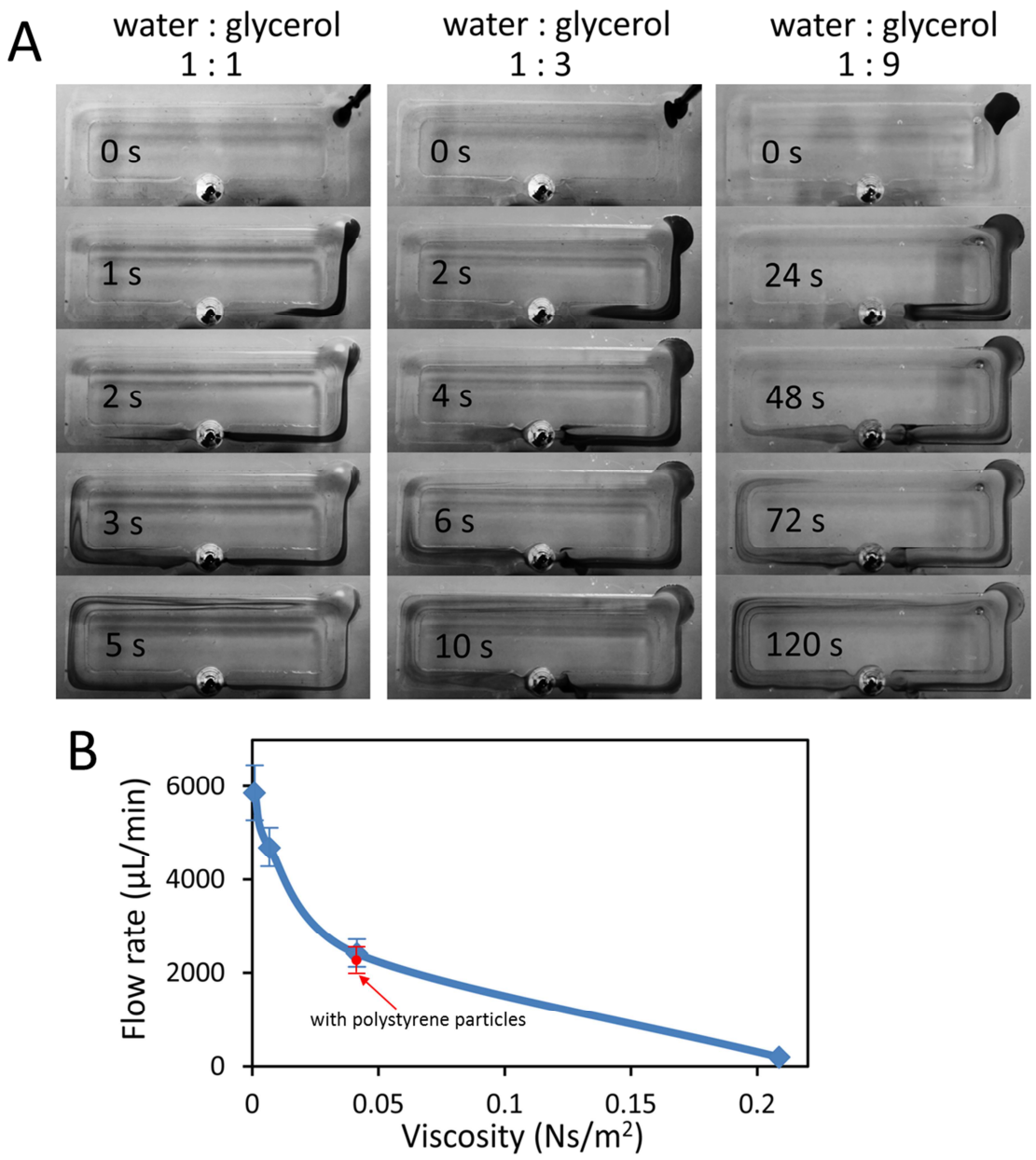

Figure S16. Pumping liquids with high viscosity. (*A*) Sequential snapshots for pumping water-glycerol solutions with the mixing ratios of 1:1, 1:3 and 1:9, while the concentration of NaOH is 0.3 mol/L. (*B*) Plot of the flow rate *vs* viscosity for water-glycerol solutions of different mixing ratios with and without polystyrene particles.

SI Appendix 17: Pump performance characterization with NaCl and PBS buffers.

We investigate the performance of the pump for pumping NaCl solution as a function of the frequency and magnitude of the square wave signal as well as the ion concentration of the solution.

Figure S17.a-A shows the variations of flow rate with respect to different frequencies. Our observations demonstrate that the highest flow rate of ~5,400 µL min^{-1} is achieved when the frequency of the square wave is set to 50 Hz. Compared to the NaOH solution, larger voltage magnitudes are required to achieve similar flow rates with the NaCl solution. At a constant frequency of 50 Hz, the flow rate increases with increasing the magnitude of the applied voltage, as shown in Fig. S17.a-B. No electrolysis of the NaCl solution is observed for voltages as large as 10 V_{p-p} when a 50 Hz square wave is applied (electrolysis is only observed for potentials larger than 11 V_{p-p}).

The pumping performance is further investigated by changing the ion concentration of the solution, as shown in Fig. S17.a-C. Similar to the pumping performance of NaOH solution, the flow rate becomes saturated when the ion concentration is higher than 0.4 mol/L.

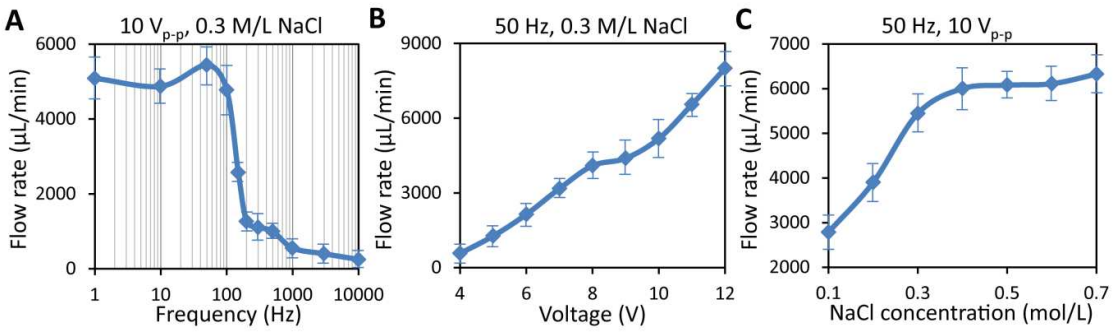

Figure S17.a. Pump performance characterization with NaCl solution. (*A*) Flow rate *vs* square wave frequency plot in a 0.3 mol/L NaCl solution. (*B*) Flow rate *vs* square wave V_{p-p} plot in a 0.3 mol/L NaCl solution. (*C*) Flow rate *vs* liquid NaCl concentration plot. Results obtained with a 2.7 mm diameter Galinstan droplet, a $V_{p-p}/2$ DC offset is always included to the voltage signals, and the duty cycle of the square wave is 50%.

Similarly, we investigate the performance of the pump for pumping PBS buffer as a function of the frequency and magnitude of the applied signal. Fig. S17.b-A shows the variations of flow rate with respect to different frequencies. Two peaks are observed at the frequencies of 1 and 50 Hz, and the highest flow rate of ~5,900 µL min^{-1} is achieved when the frequency of the square wave is set to 1 Hz. However, the solution cannot be pumped continuously when such a low frequency signal is applied and electrolysis of the solution is observed. Similar to the base solution (Supplementary S14), at a low frequency of 1 Hz, the increase of flow rate is probably due to the elongation of the droplet. For a 50 Hz square wave, no significant electrolysis of the buffer is observed when voltages as large as 12 V_{p-p} are applied (electrolysis observed for voltages larger than 14 V_{p-p}). Increasing the magnitude of the applied voltage enhances the flow rate, as shown in Fig. S17.b-B.

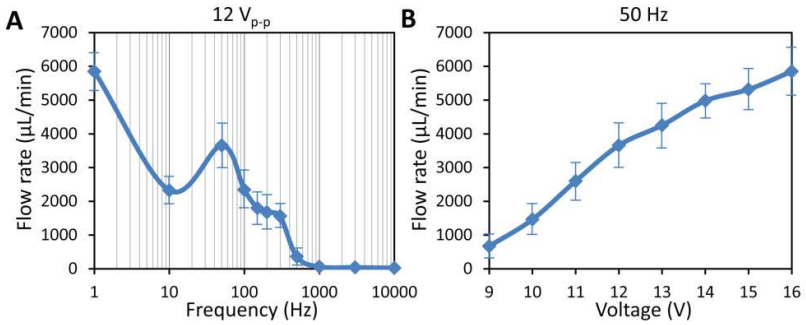

Figure S17.b. Pump performance characterization with PBS buffer. (*A*) Flow rate *vs* square wave frequency plots. (*B*) Flow rate *vs* square wave V_{p-p} plots. Results are obtained with a 2.7 mm diameter Galinstan droplet, a $V_{p-p}/2$ DC offset is always included in the voltage signals, and the duty cycle of the square wave is 50%.

We also conduct the ICP-MS test for both NaCl solution and PBS buffer after 100 pumping cycles to examine the consumption of the droplet in time and its durability. For 0.3 mol/L NaCl solution pumped with a 10 V_{p-p}, 50 Hz square wave, the results indicate that gallium and tin are dissolved at small rates, with their concentration in solution increase from 0.17 to 27.55 µmol/L for gallium, and

from 0.10 to 0.76 μmol/L for tin. Applying the same calculation procedure given in Supplementary S5, the pump is able to work continuously for at least 100 days in NaCl solution. For PBS buffer pumped with a 12 V_{p-p}, 50 Hz square wave, gallium and tin are dissolved, with the concentration increased from 2.36 to 86.96 μmol/L for gallium, and from 0.09 to 0.23 μmol/L for tin. Therefore, the pump is able to work continuously for at least 34 days in PBS buffer.

SI Appendix 18: Pumping with microfluidic channels.

In order to test the pump performance in microfluidics, we scale down the size of the channel and design a close-loop microchannel, as shown in Fig. S18. We place the PDMS microchannel with a cross section of 240×600 μm onto a PMMA substrate with a cylindrical droplet seat of diameter = 2 mm and depth = 2 mm to hold the Galinstan droplet. A Galinstan droplet with a diameter of 2 mm is placed in the droplet seat.

Under this combination, the cross sectional area of the current path ($A_{current}$) is significantly reduced (approximately 10 times less compared to the large channel shown in Fig. 1 in the main manuscript). According to Eq.**1** a much larger potential is required to generate enough pressure difference to pump the liquid. This issue can be resolved by expanding the electrode seats on the PMMA substrate to enlarge the average current path area (Fig. S18B-C). This increases the average cross-sectional area of the current path by about 3 times, and significantly reduces the magnitude of the voltage required to perform pumping.

For the close-loop microchannel, applying a square wave signal (400 Hz, 16 V_{p-p}, 8 V DC offset and 50% duty cycle) with NaOH solution (0.3 mol/L) leads to a flow rate of 70 μL/min (Fig S18-D). The 400 Hz signal frequency is chosen since it is the optimum frequency for a Galinstan droplet with a 2 mm diameter (see Supplementary S14).

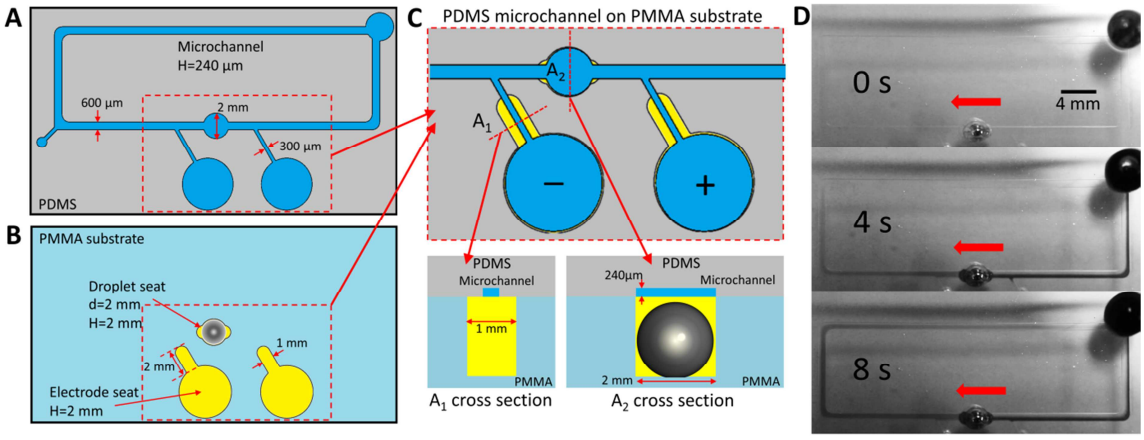

Figure S18. Experiments with the close-loop microfluidic system. (*A*) shows the close-loop PDMS microchannel system. The overall channel length is 65 mm and the gap between the electrodes is 10 mm. The height of the channel is 240 µm. (*B*) shows the design of the PMMA substrate, droplet and electrode seat with 2 mm height are fabricated by milling the substrate. (*C*) shows the area in red dash boxes of (*A*) and (*B*) after placing the PDMS channel onto the PMMA substrate. The two subsets show the cross-sectional area along the lines A_1 an A_2. (*D*) Sequential snapshots for pumping NaOH solution (0.3 mol/L) in the close-loop microchannel, while a square wave signal (400 Hz, 16 $V_{p\text{-}p}$, 8 V DC offset and 50% duty cycle) is applied. Galinstan droplet with 2 mm diameteris is used for pumping and a droplet of dye is used to demonstrate the pumping effect. Scale bar is 4 mm.

SI Appendix References

1. Lee J, Kim CJ. (1999) Theory and modeling of continuous electrowetting microactuation. *Proceedings of the ASME International Mechanical Engineering Congress and Exposition, MEMS* 1.

2. Beni G, Hackwood S, Jackel JL. (1982) Continuous electrowetting effect. *Appl Phys lett* 40:912-914.

3. White FM (2003) *Fluid Mechanics* (McGraw-Hill: Boston).

4. Zhao Y, Frost RL (2008) Raman spectroscopy and characterisation of α-gallium oxyhydroxide and β-gallium oxide nanorods. *J Raman Spectrosc* 39:1494-1501.

5. Liu T, Sen P, Kim C-J (2012) Characterization of Nontoxic Liquid-Metal Alloy Galinstan for Applications in Microdevices. *J Microelectromech Syst* 21:443-450.

6. van Ingen GN, Kapteijn J, Meijering JL (1970) On the system Gallium-Indium-Tin. *Scripta Metallurgica* 4:733-736.

7. Cheng NS (2008) Formula for the Viscosity of a Glycerol−Water Mixture. *Ind. Eng. Chem. Res.* 47: 3285-3288.